

# xTern: Energy-Efficient Ternary Neural Network Inference on RISC-V-Based Edge Systems

Georg Rutishauser\*, Joan Mihali<sup>†</sup>, Moritz Scherer\*, Luca Benini\*<sup>†</sup>

\*Departement Informationstechnologie und Elektrotechnik, ETH Zürich, Zürich, Switzerland

<sup>†</sup>Dipartimento di Ingegneria dell'Energia Elettrica e dell'Informazione, Università di Bologna, Bologna, Italy

Email: {georg.r, scheremo, lbenini}@iis.ee.ethz.ch, jmihali1997@gmail.com

**Abstract**—Ternary neural networks (TNNs) offer a superior accuracy-energy trade-off compared to binary neural networks. However, until now, they have required specialized accelerators to realize their efficiency potential, which has hindered widespread adoption. To address this, we present xTern, a lightweight extension of the RISC-V instruction set architecture (ISA) targeted at accelerating TNN inference on general-purpose cores. To complement the ISA extension, we developed a set of optimized kernels leveraging xTern, achieving 67 % higher throughput than their 2-bit equivalents. Power consumption is only marginally increased by 5.2 %, resulting in an energy efficiency improvement by 57.1 %. We demonstrate that the proposed xTern extension, integrated into an octa-core compute cluster, incurs a minimal silicon area overhead of 0.9 % with no impact on timing. In end-to-end benchmarks, we demonstrate that xTern enables the deployment of TNNs achieving up to 1.6 percentage points higher CIFAR-10 classification accuracy than 2-bit networks at equal inference latency. Our results show that xTern enables RISC-V-based ultra-low-power edge AI platforms to benefit from the efficiency potential of TNNs.

## I. INTRODUCTION

Edge systems such as Internet of Things (IoT) sensor nodes are producing ever-increasing amounts of data. Simultaneously, machine learning (ML) techniques have revolutionized the state of the art in interpreting such data, from computer vision to medical data processing. To decrease latency and communication energy, alleviate privacy concerns, and improve the versatility of sensing systems, the trend has been to move the ML-based processing of sensor data away from centralized cloud servers and onto the device that collects them, a paradigm termed “edge AI”. Thanks to their ubiquity and low cost as well as their low operating power, microcontroller (MCU)-based systems are one of the most popular targets for the deployment of edge AI applications [1]. However, MCUs also come with stringent memory and processing resource constraints, making the deployment of large, compute-intensive deep neural networks (DNNs) to these platforms highly challenging and elevating the importance of careful optimization of ML algorithms to the target hardware.

*Quantization* has proven an essential technique to optimize the efficiency of DNNs for edge deployment. By representing network parameters and intermediate activations as low-bitwidth integers rather than full-precision floating-point numbers, a model’s compute resource, storage, and memory

requirements can be decreased. Together with innovations in efficient model topologies [2], [3], research in quantization has enabled models running on sub-100 mW MCU platforms to achieve statistical performance that would have required high-performance workstations less than a decade ago [4]. Given a suitable hardware platform, the most aggressive quantization schemes offer the largest efficiency gains: In binary neural networks (BNNs), parameters and activations take values in  $\{-1, 1\}$  and are represented by a single bit, and in ternary neural networks (TNNs), they may additionally take the zero value. In the domain of extreme quantization, research on TNNs has shown that moving from binary to ternary quantization increases statistical accuracy significantly and results in superior accuracy-complexity trade-offs [5]. We illustrate this with an example in Section II-A.

In the quest for efficient inference, dedicated hardware accelerators for quantized neural networks (QNNs) of all forms, from BNNs to 8-bit and mixed-precision networks, have seen success in recent years [6], [7]. However, application-specific accelerators imply a large commitment in silicon area dedicated solely to QNN inference, which may be unacceptable for low-cost embedded systems. In such cases, implementing hardware support for low-precision arithmetic in general-purpose processing cores with custom instruction set architecture (ISA) extensions offers an attractive alternative to single-purpose accelerators. Although operational efficiency is generally lower, implementation overhead is greatly decreased, and efficiency gains over the unmodified system are substantial. ISA extensions also provide flexibility – while accelerators commonly support a finite set of layers, well-designed low-precision arithmetic instructions can be used to implement arbitrary kernels. For example, recent successes in weight ternarization of large language model (LLM) architectures [8] suggest that fully ternarized transformers may enable LLM inference on edge systems; ISA-level support for ternary arithmetic will prepare systems for these future architectures. Researchers have proposed several ISA extensions for low- and mixed-precision integer arithmetic and used them to optimize the accuracy-energy trade-off. However, while integer-bitwidth low-precision operations readily map to single instruction, multiple data (SIMD)-based ISA extensions, efficient execution of TNNs has thus far been restricted to dedicated accelerators due to their non-power-of-two value range.

J. Mihali contributed to this work in the scope of his Master’s thesis at ETH Zürich.

To overcome this limitation, we aim at achieving efficient TNN inference on RISC-V processing cores with minimal hardware overhead, enabled by a lightweight extension of the RISC-V ISA. Specifically, we present the following contributions in this paper:

- We propose xTern, a lightweight extension to the RISC-V ISA designed to enable efficient inference of TNNs. We further enable the development of end-to-end applications using xTern with an end-to-end software stack consisting of GCC compiler support, an optimized kernel library and an automated deployment flow.
- We implement the proposed instructions in an open-source RISC-V core targeted at energy-efficient edge AI applications and construct an 8-core compute cluster based on the modified architecture. We show that our modifications result in a negligible area overhead of  $< 1\%$  compared to the baseline cluster with a negligible impact on the power consumption of 8-bit applications.
- We conduct detailed performance and energy efficiency evaluations of the xTern hardware and software stack. We show that our kernels increase throughput by 67% on ternary convolutions compared to state-of-the-art 2-bit kernels. In post-layout simulations of the xTern system, we demonstrate a marginal increase in power consumption of only 5.2%, leading to an energy efficiency gain of 57%.
- We evaluate xTern's impact on inference energy efficiency on two end-to-end applications. In image classification on the CIFAR-10 dataset, we demonstrate that xTern enables the deployment of TNNs that achieve up to 1.6 percentage points (pp.) higher classification accuracy at equal inference latency compared to 2-bit QNNs. In an 11-class gesture recognition task, we demonstrate a reduction of inference energy by 33% at a negligible accuracy drop when comparing TNN inference using xTern to an optimized 2-bit QNN running on an equivalent system without our extension.

## II. BACKGROUND

### A. Ternary Neural Networks

Ternary neural networks are QNNs where all activations and weights take values in the set  $\mathcal{T} \triangleq \{-1, 0, 1\}$ . A typical convolutional TNN is composed of a series of layer stacks, each consisting of a convolutional layer followed by an element-wise non-linear activation, with an optional pooling layer between convolution and activation to decrease the spatial dimension of the output feature maps. The activation layer maps the convolution/pooling layer's integer output  $\mathbf{Z} \in \mathbb{Z}^{N_o \times H \times W}$  to ternary activations  $\mathbf{Y} \in \mathcal{T}^{N_o \times H \times W}$  by the channel-wise thresholding function  $\sigma(\cdot)$ :

$$y_{i,x,y} = \sigma(z_{i,x,y}) = \begin{cases} -1, & z_{i,x,y} < t_i^{lo} \\ 0, & t_i^{lo} \leq z_{i,x,y} < t_i^{hi} \\ 1, & z_{i,x,y} \geq t_i^{hi}, \end{cases} \quad (1)$$

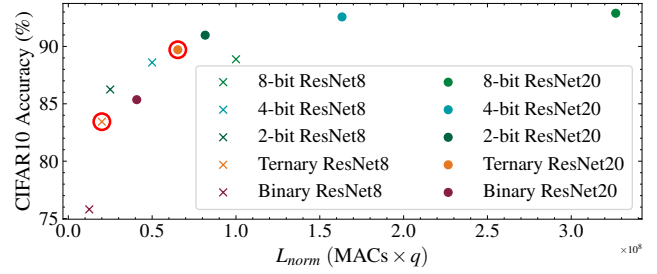


Fig. 1: Comparison of accuracy vs normalized load  $L_{norm}$  of ResNet8 and ResNet20, quantized to different precisions, on CIFAR10. Networks were trained with the TQT algorithm [10], with the first and last layers quantized to 8-bit precision. TNNs are highlighted in red.

where  $t_i^{lo}, t_i^{hi} \in \mathbb{Z}^{N_o}$  are vectors of lower and upper integer thresholds, respectively.

At first glance, TNNs are at a disadvantage in terms of network size and efficiency when compared to two-bit QNNs and BNNs: Each ternary value requires two bits of storage but only encodes  $\log_2 3 \approx 1.585$  bits of information. However, by assigning each possible sequence of 5 ternary values a distinct 8-bit string, the storage space required is reduced to 1.6 bit per value, close to the theoretical optimum. In the context of dedicated accelerators, TNNs represent a particularly attractive operating point. In [5], the authors show that a well-designed ternary accelerator can achieve better inference efficiency than an equivalent BNN accelerator on the same network topology. Ternary compression partially amortizes the memory overhead over a binary design, and the addition of a zero value allows for sparsity, which directly translates to reduced switching activity in an unrolled datapath, improving energy efficiency. At the same time, classification accuracy is improved over BNNs due to the increased representational capacity of TNNs. In contrast to application-specific accelerators, ISA-based processing cores operate on fixed-width data words. This constraint on datapath design means that the 25% increase in data density from ternary compression is crucial to maximizing the achievable performance when processing ternary data. In this paper, we choose the encoding proposed in [9] for its low-complexity hardware implementation.

*Comparison to Other QNNs:* To achieve an optimal accuracy-efficiency trade-off for a given application, a QNN must be chosen among all model architectures *and* quantization policies supported by the target hardware architecture; Figure 1 illustrates such a trade-off curve for two lightweight networks, ResNet8 (from the MLPerf Tiny Benchmark [11]) and ResNet20, on the CIFAR-10 [12] dataset. We define the *normalized load*  $L_{norm}$  posed by a  $q$ -bit QNN as the number of multiply-accumulate (MAC) operations multiplied by  $q$ , assuming SIMD execution and inverse linear scaling of throughput with bitwidth. We set  $q = 1.6$  for TNNs, assuming the use of the compression scheme described earlier. Figure 1 exemplifies that smaller networks like ResNet8, quantized to higher bit widths, may dominate larger BNNs in terms of

accuracy and inference latency. In contrast, the ResNet20 TNN extends the Pareto front, offering an attractive operating point and demonstrating the advantages of TNNs.

### B. QNN Inference on MCU-Class Platforms

To reap QNNs' efficiency potential, an inference platform must provide hardware support for their execution. Application-specific accelerators achieve the highest efficiency: BNN [6], [13] and TNN [5], [14] accelerators report efficiencies of up to 1 POp/J. Many accelerator designs for BNNs, TNNs and other low-bitwidth QNNs have been proposed, but there are fewer documented end-to-end applications deployed to such accelerators embedded in MCU-class systems. Examples include face recognition [15] and gesture recognition [16]. While they report superior energy efficiency figures, the accelerators implemented in these systems occupy a significant proportion of the total silicon area. Such a commitment of silicon resources may not be affordable for low-cost edge MCUs – indeed, most commercial edge systems only have ISA-based reduced instruction set computer (RISC) processing cores. Recent work has shown that BNNs can be efficiently executed with XOR and population count instructions [17], found in most ISAs targeting embedded and edge systems. Multiple authors have adopted this approach to implement BNN kernel libraries [18], [19] and applications such as BNN-based keyword spotting [20] on off-the-shelf MCUs without BNN-specific hardware.

In contrast to BNNs, the efficient execution of QNNs in general and TNNs in particular on ISA-based processing cores poses significant challenges. Mainstream ISAs have limited support for arithmetic on sub-word data types, severely limiting the potential efficiency gains, as data packing and unpacking has to be implemented in software. In commercial MCUs based on the ARMv8.1 ISA, native support for sub-word arithmetic has been addressed for 8-bit and 16-bit operands by packed-SIMD MAC instructions [21].

While 8-bit QNNs achieve full-precision equivalent accuracy with the use of quantization-aware training algorithms [22], [23], sub-byte and mixed-precision quantization enable even higher efficiency and a finer-grained trade-off between inference energy and statistical accuracy. Multiple works have proposed extensions to the open RISC-V ISA targeted at QNN inference. BISDU [24] proposes extensions accelerating the bit-serial computation of sub-byte arithmetic operations, targeting minimum silicon area overhead. As we aim for maximum throughput at the best possible efficiency, we base the present work on XpulpNN [25]. XpulpNN extends the RISC-V ISA by adding support for 4-bit and 2-bit data types through packed-SIMD instructions. Furthermore, it mitigates the von Neumann bottleneck by fusing computation and data access into MAC-and-load (M&L) operations. Input activations and weights are read from an additional 2-port register file (RF), the NN-RF. Combining a SIMD MAC operation with the loading of the next activation or weight word and the update of the corresponding pointer enables optimized kernels to eliminate most explicit loads and pointer arithmetic, with

the utilization of arithmetic units reaching up to 94 %. The XpulpNN ISA extension further encompasses the XpulpV2 ISA, which implements instructions to decrease memory management and control flow overhead, such as post-increment load and stores and hardware loops, further increasing QNN inference efficiency.

## III. THE RISC-V xTERN ISA EXTENSION

In the following, we describe the xTern ISA extension, its integration into an 8-core cluster of high-performance RISC-V cores, and the software infrastructure to enable its use in end-to-end edge AI applications.

### A. Instructions

xTern extends the 32-bit RISC-V ISA. It is a very compact extension, consisting of three types of instructions which cover all operations required to execute the different layers of a TNN. All xTern instructions consume or produce ternary data elements, using the compression scheme proposed in [9] to represent 5 ternary elements (trits) with one byte or 20 trits with a 32-bit word. TNN layers can be mapped to kernels using three types of xTern instructions: multiply-add (MADD) instructions, element-wise comparison instructions and the threshold-and-compress instruction. All instructions are only implemented for signed ternary elements, as networks with unsigned activations can be converted to signed as shown in [16]. Figure 3a shows the encoding of the instructions introduced by xTern.

**MADD Instructions:** The dot products in linear operators such as convolutions are implemented with MADD instructions, which perform 20-way packed-SIMD MAC operations on two input words, producing a 32-bit integer result. xTern implements three instructions of this class, all using the same hardware unit to perform the multiply-add operation, shown in Figure 2b. `dotsp.t` performs a pure MADD of `rs1` and `rs2` (operands A and B in Figure 2b), storing the result in `rd`. The `sdotsp.t` instruction performs the analogous MAC operation, adding the MADD result to the contents of `rd`. The `mlsdotsp.t` instruction extends XpulpNN, performing a MAC-and-load operation. The MADD input operands are taken from the NN-RF, and `rd` is used as an accumulator. Its operation and encoding is implemented analogously to the 2-bit, 4-bit and 8-bit M&L instructions implemented by XpulpNN, which are described in detail in [25].

**Element-wise Comparison Instructions:** Element-wise comparison instructions take two compressed 20-element input words, comparing each element between both and storing a compressed word of the smaller (`min.t`) or larger (`max.t`) element at each position into the destination register. The `max.t` instruction can be used to implement max-pooling layers efficiently.

**Threshold-and-Compress Instruction:** Activation layers in TNNs are implemented with thresholding operations, which can be mapped to xTern's *threshold-and-compress* instruction (`thrc`). It takes three registers as inputs: `rs1` contains a 32-bit integer number, which is compared with two 16-bit integer

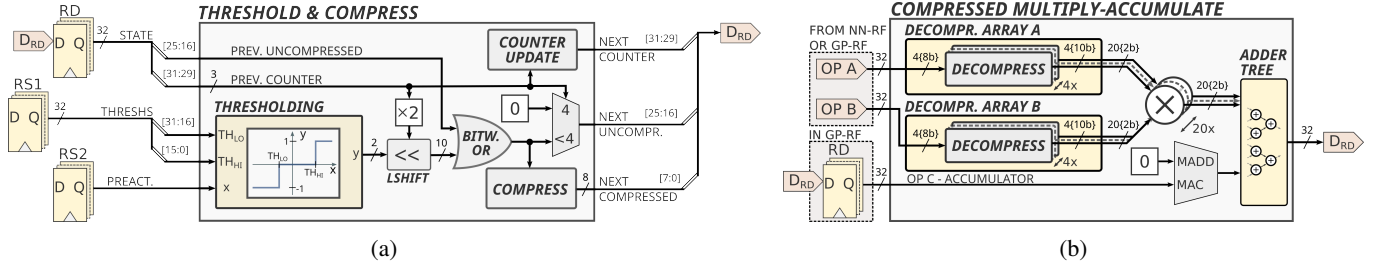


Fig. 2: Schematic of the hardware for the threshold-compress (`thrc`, shown in a) and compressed MAC (`smldotsp.t`, `sdotsp.t`, shown in b) instructions.

31	25:24	20:19	15:14	12:11	7	6	0	
1111100	IMM	rs1	100	rd	1110111			<code>smldotsp.t</code>
1011101	rs2	rs1	100	rd	1010111			<code>sdotsp.t</code>
1001101	rs1	rs1	100	rd	1010111			<code>dotsp.t</code>
0010001	rs2	rs1	100	rd	1010111			<code>min.t</code>
0011001	rs2	rs1	100	rd	1010111			<code>max.t</code>
0000100	rs2	rs1	110	rd	0110011			<code>thrc</code>

(a) Encoding of xTern instructions

31	29:28	26:25	16:15	8	7	0	
$c$	0	$x_{uncompr}$	0	$x_{compr}$			<code>rd</code>
$t^{lo}$				$t^{hi}$			<code>rs1</code>

(b) Encoding of `thrc` status (`rd`) and threshold (`rs1`) registers

Fig. 3: Encoding of instructions and input/output registers of xTern instructions

thresholds stored in `rs2` to produce a ternary result. As the ternary compression encodes five trits into an 8-bit value and thresholding only produces one trit, the instruction is designed in a stateful manner. `rd` serves both as an input and output register, holding the instruction’s state. The state consists of 3 items: 10 bits containing up to 5 packed, uncompressed 2-bit trits, 8 bits containing the compressed representation of those trits, and a 3-bit counter indicating how many trits have been processed already. When the instruction is executed at a counter value of  $c$ , the thresholding result is extended to a 10-bit value and left-shifted by  $2c$  bits. The shifted value is then merged with the previous uncompressed values by a bitwise OR operation, and the result is fed into a ternary compression unit. The compressed byte is stored in the updated status register, along with the next counter value and the uncompressed vector, which is reset to all-zeros after five elements have been processed. Figure 2a shows the hardware implementation of the threshold-and-compress instruction.

### B. The xTern System

To evaluate the performance and efficiency of xTern, we integrated the ISA extension into the open-source RISCY-NN core, which implements the base RV32IMC ISA and the XpulpV2 [26] and XpulpNN [25] extensions. This core

represents the state of the art for efficient QNN inference [27]. It possesses the hardware infrastructure to support M&L instructions, making it both a highly optimized comparison baseline and an ideal starting point for implementing the proposed extensions. We use the xTern-enabled RISCY core to assemble a fully-featured, high-performance, low-power system-on-chip (SoC) on which we perform our evaluations.<sup>1</sup> The system has two main processing domains: the *SoC domain* and the *cluster domain*.

A RISCY core manages system operation in the SoC domain, called the *fabric controller (FC)*. The system’s main program and data memory, termed L2 memory, is also located in the SoC domain and consists of 1 MiB of SRAM, divided into eight banks. The system’s main interconnect links the FC, on-chip peripherals, L2 memory, and the cluster domain.

Compute-intensive parallelizable tasks are offloaded to the cluster domain. It contains a parallel ultra-low power (PULP) cluster of 8 RISCY cores with 128 KiB of L1 scratchpad tightly-coupled data memory (TCDM) in 16 banks, connected with a single-cycle logarithmic interconnect to minimize data access latency. Cluster cores execute program code stored in L2 memory, which is located in a different clock domain and accessible via a 64-bit AXI4 port through a clock domain crossing (CDC). A shared instruction cache of 4 KiB minimizes stalls caused by instruction fetching through this CDC. The cluster is programmed in the single program, multiple data (SPMD) model, i.e., all cores execute the same program, using the core index to control program flow.

### C. xTern Software Support

To make the deployment of TNNs to xTern-enabled RISC-V systems accessible to application developers, we have implemented an end-to-end deployment pipeline. It consists of compiler support for the new instructions, a library of performance-optimized, parallelized kernels leveraging xTern, and a mapping tool that takes an ONNX representation of a TNN and generates a C application which executes the network.

**GCC Compiler Support:** All xTern instructions can be inferred from pure C code by calling built-in functions. This removes the need for inline assembly code and enables GCC’s full range of optimizations during the compilation process. The

<sup>1</sup>Available at <https://github.com/da-gazzi/pulp-xpulptnn/tree/xpulptnn>

modified version of GCC supporting xTern is available open source<sup>2</sup>.

**Kernel Support:** We have implemented a set of optimized ternary layer kernels leveraging xTern. They implement four layers, all operating on compressed ternary inputs: 2-dimensional convolutions, 1-dimensional dilated convolutions, max-pooling, and fully-connected layers. The fully connected kernel is intended for classifier layers that compute class scores and produces integer outputs, while the other kernels use the `thrc` instruction to produce compressed ternary outputs. The number of ternary input and output channels is restricted to multiples of 5, as the ternary compression encodes blocks of 5 elements in one byte.

As convolutional layers constitute most of the workload in DNNs, a well-optimized convolution kernel is crucial to end-to-end efficiency. Our ternary convolutional kernels take inspiration from the open-source PULP-NN library [28] and decompose convolutions into a data reordering step (*im2col*) and a matrix multiplication step (*matmul*). The matrix multiplication kernels use the `smlsdotsp` M&L instructions to perform the dot product operations, and the integer results must then be mapped back to quantized values in an additional step merging activation, batch normalization, and requantization [29]. The instructions introduced by xTern increase efficiency by optimizing both steps. The 25 % increase in data density afforded by the ternary compression directly translates to a corresponding increase of throughput in the hot loop that calculates the integer dot products. In integer-bitwidth QNNs, the activation-requantization step consists of an affine transformation followed by an arithmetic shift and data packing, taking up a significant share of the total kernel execution time. xTern’s `thrc` instruction performs the complete process in a single instruction, minimizing this overhead. Combined, these improvements lead to an increase in throughput over PULP-NN’s 2-bit kernels by much more than the 25 % that the increased data density provides, as detailed in Section IV-C.

#### D. Deployment Pipeline

For the seamless deployment of full networks to xTern-enabled systems, we have integrated support for TNNs and our xTern kernels into the open-source DORY [30] tool. DORY takes precision-annotated ONNX graphs as input and produces compilable C applications executes the network on the target platform. Multi-level memory hierarchies are supported by tiling layers that do not fully fit into the scratchpad memory. DORY uses integer linear programming (ILP) to optimize the tiling policy and inserts the appropriate DMA driver calls for data transfer between the different levels of the memory hierarchy.

### IV. RESULTS AND DISCUSSION

In this section, we evaluate the efficiency and performance of xTern. We first present hardware results collected on a full backend layout of the xTern-enabled PULP cluster. This implementation is used to evaluate the silicon area overhead and

TABLE I  
Hardware figures of merit for the xTern system and the baseline implementing only XpulpNN.

		XpulpNN	xTern (this work)
Core	$A_{core}$ <sup>a</sup>	163.5 kGE	168.4 kGE (+3.0 %)
	$P_{MM,8b}$ <sup>b</sup>	4.1 mW	4.2 mW (+2.4 %)
	$P_{Conv,LP}$ <sup>c</sup>	4.0 mW	4.3 mW (+7.8 %)
Cluster	$A_{clus}$ <sup>a</sup>	3.29 MGE	3.32 MGE (+0.9 %)
	Density	70.2 %	71.0 % (+0.8 pp.)
	$f_{clk}$ <sup>b</sup>	500 MHz (376 MHz)	500 MHz (389 MHz)
	$P_{MM,8b}$ <sup>c</sup>	58.1 mW	58.9 mW (+1.4 %)
	$P_{Conv,LP}$ <sup>c</sup>	57.7 mW	60.7 mW (+5.2 %)
	$Eff_{Conv,LP}$ <sup>c</sup>	383.9 GOP/J	603.3 GOP/J (+57.1 %)

<sup>a</sup> Obtained from synthesized netlists. One gate equivalent (GE) in 22 nm FDX is 0.199  $\mu m^2$ , the size of a NAND2 gate.

<sup>b</sup> The first number is obtained at HV operating conditions ( $V_{DD} = 0.72$  V,  $T = 25^\circ C$ ), the number in parentheses is obtained at LV operating conditions ( $V_{DD} = 0.65$  V,  $T = 25^\circ C$ ).

<sup>c</sup> Evaluated at LV operating conditions.

compare power consumption in post-layout simulations to the baseline XpulpNN cluster. We then evaluate the performance of the ternary kernels on a comprehensive benchmark suite and compare the efficiency to that of 2-bit kernels. Finally, we compare TNNs mapped to the xTern system with 2-bit networks executed on the baseline system on two end-to-end benchmark applications to evaluate xTern’s impact on the trade-off between accuracy and inference latency and energy.

#### A. Experimental Setup

For our hardware evaluations, we synthesized the 8-core PULP cluster described in Section III-B in the GlobalFoundries 22 nm FDX process, using libraries for the typical corner with  $V_{DD} = 0.8$  V. We used Synopsys Design Compiler 2019.3 and constrained the core clock to a period  $t_{clk} = 1.5$  ns. We used the synthesized netlist to perform a full backend layout using Cadence Innovus 21.13. We optimize for two supply voltages,  $V_{DD} = 0.72$  V (HV, max. throughput) and  $V_{DD} = 0.65$  V (LV, max. efficiency). We target a system clock frequency of  $f_{clk} = 500$  MHz; the achieved frequencies are listed in Table I. The synthesis and backend layout flow is identical for both cluster versions. Power results were generated by simulating the full system using the post-layout netlists of the two cluster implementations to collect value change dump (VCD) files, which were used to estimate the power consumption in Innovus. We ran performance evaluations on an FPGA port of the complete system, generated from the same SystemVerilog RTL code as the physical implementation.

#### B. Hardware Impact

To evaluate the implementation overhead of our extension, we compare the silicon area and timing of the 8-core cluster implementing xTern to an identically parametrized baseline cluster implementing only the XpulpV2 and XpulpNN extensions. This baseline represents the state of the art in AI-targeted, RISC-V-based MCU-class systems. The overhead we report thus reflects the cost of adding TNN optimizations to a system already intended for inference of QNNs. Table I

<sup>2</sup><https://github.com/da-gazzi/pulp-tnn-gnu-toolchain>



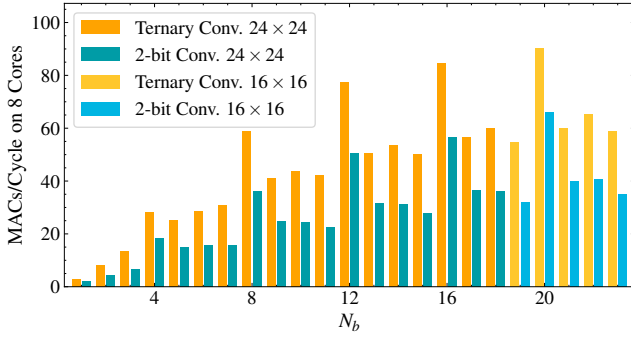


Fig. 4: Throughput comparison between ternary convolution kernels and 2-bit kernels from the PULP-NN on the 8-core PULP cluster.

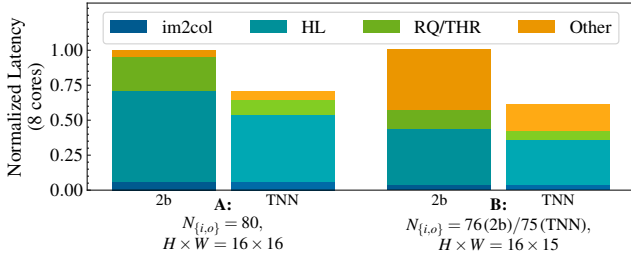


Fig. 5: Latency breakdown comparison between 2-bit and ternary  $3 \times 3$  convolution kernels. Latency is normalized to the 2-bit kernel’s latency and is decomposed into *im2col*, *hot loop* (HL), *requantization/thresholding* (RQ/THR) and *Other* components and shown for two test cases.

reports the standard cell areas  $A_{\{core,clus\}}$  after synthesis, the achieved operating frequency, and the power consumption.  $P_{conv,LP}$  denotes power consumption of 2-bit convolution on the baseline system and ternary convolution on the xTern system.  $P_{MM,8b}$  is the power consumption during 8-bit matrix multiplication, an indicator of the impact of our modifications on cluster power consumption for programs that do not use the new instructions. We report these figures both for a single core and the complete cluster. The area overhead of xTern on a single core is already low at 3 %. At 0.9 %, the cluster-level overhead is even lower, as our modifications do not affect the other components of the cluster, such as L1 memory and instruction cache. Timing is not impacted since the critical path in both cluster versions is in the floating-point unit (FPU). The negligible area increase and non-existent timing impact mean that the addition of xTern essentially incurs zero implementation overhead when placing and routing the cluster. This assessment is confirmed by the negligible post-route standard cell density increase of 0.8 percentage points.

### C. Kernel Performance and Efficiency

Figure 4 shows the throughput of ternary (using our kernels, optimized for xTern) and 2-bit (using PULP-NN kernels optimized for XpulpNN) convolutions running on eight cores.  $N_b$  is the number of bytes required to store all  $N_{\{i,o\}}$  input/output

TABLE II

Architecture of VGG-like networks used in end-to-end latency evaluation on CIFAR-10 dataset.  $(C\{1/2\}D\{S/V/C\})$ : 1/2-dimensional convolution with same/valid/causal padding. **MP**: Max-pooling layer. **FC**: fully-connected layer. MP layers use a  $2 \times 2$  kernel, a stride of 2 and no padding. The channel count of convolutional layers  $N_c$  is parametrizable; we evaluate  $N_c \in \{32, 48, 64, 80, 96\}$  (2b QNNs) and  $N_c \in \{40, 60, 80, 100\}$  (TNNs).

Layer	Outp. Res.	$C_{out}$	$k_{conv}$	$b_w^a$	$b_o^a$
Input	$32 \times 32$	3	$3 \times 3$	–	8
C2D(S)-MP	$16 \times 16$	32	$3 \times 3$	8	1.6/2
C2D(S)	$16 \times 16$	$N_c$	$3 \times 3$	1.6/2	1.6/2
C2D(S)-MP	$8 \times 8$	$N_c$	$3 \times 3$	1.6/2	1.6/2
C2D(S)	$8 \times 8$	$N_c$	$3 \times 3$	1.6/2	1.6/2
C2D(S)-MP	$4 \times 4$	$N_c$	$3 \times 3$	1.6/2	8
FC	1	10	–	8	32

<sup>a</sup> Weight/output precision in bits; 1.6 denotes ternary precision

channels of a single pixel, with  $N_i = N_o = 5N_b$  for ternary kernels and  $N_i = N_o = 4N_b$  for 2-bit kernels. The kernel size is  $k \times k = 3 \times 3$ , and the input and output feature map sizes are chosen such that inputs, outputs, and weights fit into L1 memory. On average, ternary kernels achieve 67 % higher throughput than 2-bit kernels at equal  $N_b$  and resolution. When restricting the comparison to layers where the channels of each pixel fill an integer number of 32-bit words, i.e.,  $N_b = 4k$ ,  $k \in \mathbb{Z}$ , the ternary kernels exhibit 51 % higher throughput than their 2-bit equivalents. Those layers also stand out for their considerably higher throughput, as all dot product calculations can be performed in the optimized matrix multiplication hot loop. Figure 5 illustrates the nature of the speedup afforded by xTern. In test case A, all pixels are word-aligned, and all calculations are performed in the optimized hot loop, which accounts for most of the latency in the 2-bit kernel together with the requantization step. The ternary kernels reduce hot loop and requantization latency by 27 % and 55 %, respectively, resulting in an overall latency reduction by 30 %. The latency from the other contributors is roughly equal to the 2-bit kernel. In test case B, pixels are not word-aligned. The ternary kernels’ optimized handling of leftover calculations yields a latency reduction of 38 % after scaling the latency to the slightly reduced number of MACs performed. Thanks to this increased throughput and the low power consumption overhead, ternary convolutions on an equal data volume on the xTern system are 57 % more efficient than 2-bit convolutions on the baseline system, placing TNNs at a very attractive trade-off point of accuracy and energy consumption.

### D. End-to-End Network Inference

To evaluate how xTern can be used in end-to-end edge applications, we consider two benchmark tasks. The first is 11-class gesture recognition on dynamic vision sensor (DVS) data from the DVS128 dataset [31], and the second is image classification on the popular CIFAR-10 dataset [12]. On both tasks, we compare optimized 2-bit QNNs and TNNs mapped to the xTern system using our deployment pipeline.

**CIFAR-10 Image Classification:** We evaluate the trade-off between latency and classification accuracy for 2-bit and

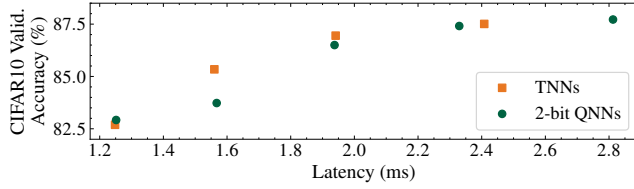


Fig. 6: Latency comparison of VGG-like networks quantized to 2-bit and ternary precision.

TABLE III

Architecture of the DVS gesture classification networks used for evaluation. *S*: Stride, *D*: Dilation. Other notation and parametrization as in Table II.

	Layer	Outp. Res.	$C_{out}$	$k_{conv}$	$D$	$S$
2D CNN	Input	$64 \times 64$	4	—	—	—
	C2D(S)-MP	$32 \times 32$	$N_{c,1}$	$3 \times 3$	1	1
	C2D(S)-MP	$16 \times 16$	80	$3 \times 3$	1	1
	C2D(S)-MP	$8 \times 8$	80	$3 \times 3$	1	1
	C2D(S)-MP	$4 \times 4$	80	$3 \times 3$	1	1
	C2D(V)-MP	$1 \times 1$	80	$3 \times 3$	1	1
1D TCN	C1D(C)	$1 \times 5$	80	2	1	1
	C1D(C)	$1 \times 5$	80	2	2	2
	C1D(C)	$1 \times 5$	80	2	4	4
	FC	$1 \times 1$	11	—	—	—

ternary networks on the example of a small VGG-like network architecture. The architecture is detailed in Table II. The first and last layers are trained and executed in 8-bit precision, all other layers are in 2-bit or ternary precision. We scale the networks by adjusting the number of input and output channels of all layers after the first, which is fixed to 32 output channels. As our ternary kernels do not support this number of input channels, the output of the first layer is zero-padded to 40 channels for the TNNs. We use our deployment flow to map the networks to the xTern system, using a cluster clock frequency of 300 MHz. Figure 6 shows the accuracy-latency trade-off for the 4 different TNN and 5 different 2-bit QNN parametrizations. All evaluated TNNs extend the accuracy-latency Pareto front, with the 60-channel TNN achieving a 1.6pp. higher validation accuracy than the 48-channel 2-bit network at a marginally lower latency.

**DVS Gesture Recognition:** We adopt the hybrid network architecture proposed in [16], consisting of a 2-dimensional convolutional neural network (CNN) followed by a 1-dimensional temporal convolutional network (TCN). The 2D CNN takes an input image of  $64 \times 64$  pixels with 4 channels, where each channel represents a DVS event frame. DVS event frames are natively ternary, as the sensor can report a positive/negative event ( $\pm 1$ ) or no event at all (0) during a time window; this makes DVS data particularly suited for processing with TNNs. The architecture of the network is detailed in Table III. For a fair comparison between 2-bit QNNs and TNNs, the layers of 2-bit networks must have multiples of 16 input channels, while TNN layers should have multiples of 20 input channels, so that feature map pixels are word-aligned and kernel performance is optimal (see Figure 4). We achieve this by slightly modifying the architecture from [16].

TABLE IV

Comparison of end-to-end inference performance between 2-bit and ternary networks on DVS gesture recognition networks.

$N_{c,1}$	2-bit QNN		TNN
	32	16	20
<b>DVS128 Acc.</b>	96.5 %	96.0 %	96.2 % (−0.3 pp.)
<b>MACs</b>	47.9M	33.7M	37.2M
$t_{inf}$	5.7 ms	4.1 ms (−27.7 %)	3.6 ms (−37.4 %)
$\Theta$ (MACs/Cyc.)	28.0	27.2 (−2.7 %)	34.8 (+24.3 %)
$E_{inf,cl}^a$	329 $\mu$ J	238 $\mu$ J (−28 %)	217 $\mu$ J (−33 %)

<sup>a</sup> Estimated from post-layout power simulation results

We change all layers but the first to have 80 input and output channels, the smallest common multiple of 16 and 20. As the first layer’s large input resolution incurs a high computation cost that scales with the number of its output channels  $N_{c,1}$ , we set  $N_{c,1} = 20$  for the TNN, and evaluate 2 settings ( $N_{c,1} = 16$  and  $N_{c,1} = 32$ , as originally described in [16]) for the 2-bit QNN. Inference latency, energy and validation accuracy results are shown in Table IV. Compared to the large baseline 2-bit QNN, the TNN exhibits 37.4 % lower inference latency and an estimated 33 % lower inference latency at a negligible accuracy drop of 0.3 pp.. Compared to the reduced-size 2-bit network, which has approximately 10 % fewer operations, the TNN’s latency and inference energy are still lower by 13.5 % and 9 %, respectively, while the validation accuracy is improved by 0.2 pp.

## V. CONCLUSION

In this paper, we address the gap between existing TNN systems, which primarily rely on dedicated accelerators, and popular edge computing systems, which are based on RISC cores with area-efficient ISA extensions. Specifically, we describe the implementation of xTern, an extension to the RISC-V ISA designed to enable the efficient processing of TNNs, in an open-source RISC-V core targeted at edge AI applications and assemble an 8-core cluster from the extended core.

A complete implementation in an IoT-friendly GF 22 nm FD-SOI technology shows that xTern incurs negligible area overhead of only 3 % and 0.9 % at the core and cluster levels, respectively, with no timing degradation. In post-layout simulations, the cluster’s power consumption while running a ternary convolution kernel is only 5.2 % higher than the baseline system running an equivalent 2-bit convolution, while our optimized kernels achieve 67 % higher throughput. This results in 57 % higher energy efficiency. In end-to-end evaluations, we show that TNNs deployed to the xTern-enabled system offer a competitive trade-off between inference latency/energy and accuracy, achieving up to 1.6pp. higher CIFAR-10 accuracy than a 2-bit QNN at equal latency. For a gesture recognition application, xTern enables the deployment of a TNNs that decreases inference latency and energy by 37 % and 33 % from a 2-bit baseline at a negligible accuracy loss of 0.3 pp.. Overall, our results show that xTern enables efficient TNN inference on RISC-V cores at negligible overhead to system implementation, posing no barrier to the adoption of our extension in edge computing systems.

## ACKNOWLEDGEMENTS

This work is supported in part by the NeuroSoC project, funded under Horizon Europe Grant Agreement n° 101070634.

## REFERENCES

- [1] R. David, J. Duke, A. Jain, V. Janapa Reddi, N. Jeffries, J. Li, N. Kreeger, I. Nappier, M. Natraj, T. Wang, P. Warden, and R. Rhodes, "TensorFlow Lite Micro: Embedded Machine Learning for TinyML Systems," in *Proceedings of Machine Learning and Systems*, A. Smola, A. Dimakis, and I. Stoica, Eds., vol. 3, 2021, pp. 800–811.
- [2] A. Howard, M. Sandler, B. Chen, W. Wang, L.-C. Chen, M. Tan, G. Chu, V. Vasudevan, Y. Zhu, R. Pang, H. Adam, and Q. Le, "Searching for MobileNetV3," in *2019 IEEE/CVF International Conference on Computer Vision (ICCV)*. IEEE, Oct. 2019, pp. 1314–1324.
- [3] M. Tan and Q. V. Le, "EfficientNet: Rethinking model scaling for convolutional neural networks," in *36th International Conference on Machine Learning, ICML 2019*, Jun. 2019, pp. 10 691–10 700.
- [4] J. Lin, W.-M. Chen, H. Cai, C. Gan, and S. Han, "Memory-Efficient Patch-Based Inference for Tiny Deep Learning," in *Advances in Neural Information Processing Systems*, A. Beygelzimer, Y. Dauphin, P. Liang, and J. W. Vaughan, Eds., Dec. 2021.
- [5] M. Scherer, G. Rutishauser, L. Cavigelli, and L. Benini, "CUTIE: Beyond PetaOp/s/W Ternary DNN Inference Acceleration With Better-Than-Binary Energy Efficiency," *IEEE Transactions on Computer-Aided Design of Integrated Circuits and Systems*, vol. 41, no. 4, pp. 1020–1033, Apr. 2022.
- [6] B. Moons, D. Bankman, L. Yang, B. Murmann, and M. Verhelst, "Binareye: An always-on energy-accuracy-scalable binary CNN processor with all memory on chip in 28nm CMOS," in *2018 IEEE Custom Integrated Circuits Conference (CICC)*. IEEE, Apr. 2018, pp. 1–4.
- [7] Y. Umuroglu, L. Rasnayake, and M. Sjalander, "BISMO: A Scalable Bit-Serial Matrix Multiplication Overlay for Reconfigurable Computing," in *2018 28th International Conference on Field Programmable Logic and Applications (FPL)*. IEEE, Aug. 2018, pp. 307–3077.
- [8] S. Ma, H. Wang, L. Ma, L. Wang, W. Wang, S. Huang, L. Dong, R. Wang, J. Xue, and F. Wei, "The Era of 1-bit LLMs: All Large Language Models are in 1.58 Bits," *arXiv preprint arXiv:2402.17764*, pp. 1–8, Feb. 2024.
- [9] O. Muller, A. Prost-Boucle, A. Bourge, and F. Petrot, "Efficient de-compression of binary encoded balanced ternary sequences," *IEEE Transactions on Very Large Scale Integration (VLSI) Systems*, vol. 27, no. 8, pp. 1962–1966, 2019.
- [10] S. R. Jain, A. Gural, M. Wu, and C. H. Dick, "Trained Quantization Thresholds for Accurate and Efficient Fixed-Point Inference of Deep Neural Networks," in *Proceedings of Machine Learning and Systems*, 2020, pp. 112–128.
- [11] C. Banbury, V. J. Reddi, P. Torelli, J. Holleman, N. Jeffries, C. Kiraly, P. Montino, D. Kanter, S. Ahmed, D. Pau, and Others, "MLPerf Tiny Benchmark," *Proceedings of the Neural Information Processing Systems Track on Datasets and Benchmarks*, 2021.
- [12] A. Krizhevsky, "Learning Multiple Layers of Features from Tiny Images," 2009.
- [13] H. Valavi, P. J. Ramadge, E. Nestler, and N. Verma, "A Mixed-Signal Binarized Convolutional-Neural-Network Accelerator Integrating Dense Weight Storage and Multiplication for Reduced Data Movement," in *2018 IEEE Symposium on VLSI Circuits*. IEEE, Jun. 2018, pp. 141–142.
- [14] S. Jain, S. K. Gupta, and A. Raghunathan, "TiM-DNN: Ternary In-Memory Accelerator for Deep Neural Networks," *IEEE Transactions on Very Large Scale Integration (VLSI) Systems*, vol. 28, no. 7, pp. 1567–1577, Jul. 2020.
- [15] P. Jokic, S. Emery, and L. Benini, "Battery-Less Face Recognition at the Extreme Edge," *IEEE New Circuits Syst. Conf.*, pp. 2–5, 2021.
- [16] G. Rutishauser, M. Scherer, T. Fischer, and L. Benini, "7  $\mu$ J/inference end-to-end gesture recognition from dynamic vision sensor data using ternarized hybrid convolutional neural networks," *Future Generation Computer Systems*, p. 109231, Jul. 2023.
- [17] M. Rastegari, V.-n. Ordonez, J. Redmon, and A. Farhadi, "XNOR-Net: ImageNet Classification Using Binary Convolutional Neural Networks," in *Lecture Notes in Computer Science (including subseries Lecture Notes in Artificial Intelligence and Lecture Notes in Bioinformatics)*, 2016, vol. 9908 LNCS, pp. 525–542.
- [18] F. Sakr, R. Berta, J. Doyle, H. Younes, A. De Gloria, and F. Bellotti, "Memory Efficient Binary Convolutional Neural Networks on Micro-controllers," *Proceedings - IEEE International Conference on Edge Computing*, vol. 2022-July, pp. 169–177, 2022.
- [19] L. Geiger and P. Team, "Larq: An Open-Source Library for Training Binarized Neural Networks," *Journal of Open Source Software*, vol. 5, no. 45, p. 1746, 2020.
- [20] G. Cerutti, L. Cavigelli, R. Andri, M. Magno, E. Farella, and L. Benini, "Sub-mW Keyword Spotting on an MCU: Analog Binary Feature Extraction and Binary Neural Networks," *IEEE Transactions on Circuits and Systems I: Regular Papers*, vol. 69, no. 5, pp. 2002–2012, 2022.
- [21] Arm Ltd., *Armv8-M Architecture Reference Manual*, Arm Ltd., 2022, available at <https://developer.arm.com/documentation/ddi0553/bw/?lang=en>.
- [22] S. K. Esser, J. L. McKinstry, D. Bablani, R. Appuswamy, and D. S. Modha, "Learned Step Size Quantization," in *International Conference on Learning Representations*, Feb. 2020, pp. 1–12.
- [23] J. Choi, S. Venkataramani, V. V. Srinivasan, K. Gopalakrishnan, Z. Wang, and P. Chuang, "Accurate and Efficient 2-bit Quantized Neural Networks," in *Proceedings of Machine Learning and Systems*, A. Talwalkar, V. Smith, and M. Zaharia, Eds., vol. 1, 2019, pp. 348–359.
- [24] D. Metz, V. Kumar, and M. Sjalander, "BISDU: A Bit-Serial Dot-Product Unit for Microcontrollers," *ACM Transactions on Embedded Computing Systems*, Jul. 2023.
- [25] A. Garofalo, G. Tagliavini, F. Conti, L. Benini, and D. Rossi, "XpulpNN: Enabling Energy Efficient and Flexible Inference of Quantized Neural Networks on RISC-V Based IoT End Nodes," *IEEE Transactions on Emerging Topics in Computing*, vol. 9, no. 3, pp. 1489–1505, Jul. 2021.
- [26] M. Gautschi, P. D. Schiavone, A. Traber, I. Loi, A. Pullini, D. Rossi, E. Flamand, F. K. Gurkaynak, and L. Benini, "Near-Threshold RISC-V Core With DSP Extensions for Scalable IoT Endpoint Devices," *IEEE Transactions on Very Large Scale Integration (VLSI) Systems*, vol. 25, no. 10, pp. 2700–2713, Oct. 2017.
- [27] M. Scherer, M. Eggmann, A. D. Mauro, A. S. Prasad, F. Conti, D. Rossi, J. T. Gómez, Z. Li, S. S. Sarwar, Z. Wang, B. D. Salvo, and L. Benini, "Siracusa: A Low-Power On-Sensor RISC-V SoC for Extended Reality Visual Processing in 16nm CMOS," in *49th European Solid State Circuits Conference (ESSCIRC)*. IEEE, Sep. 2023, pp. 217–220.
- [28] A. Garofalo, M. Rusci, F. Conti, D. Rossi, and L. Benini, "Pulp-NN: Accelerating quantized neural networks on parallel ultra-low-power RISC-V processors," *Philosophical Transactions of the Royal Society A: Mathematical, Physical and Engineering Sciences*, vol. 378, no. 2164, 2020.
- [29] M. Rusci, A. Capotondi, and L. Benini, "Memory-Driven Mixed Low Precision Quantization for Enabling Deep Network Inference on Microcontrollers," in *Proceedings of Machine Learning and Systems*, I. Dhillon, D. Papailiopoulos, and V. Sze, Eds., vol. 2, 2020, pp. 326–335.
- [30] A. Burrello, A. Garofalo, N. Bruschi, G. Tagliavini, D. Rossi, and F. Conti, "DORY: Automatic End-to-End Deployment of Real-World DNNs on Low-Cost IoT MCUs," *IEEE Transactions on Computers*, vol. 70, no. 8, pp. 1253–1268, Aug. 2021.
- [31] A. Amir, B. Taba, D. Berg, T. Melano, J. McKinstry, C. Di Nolfo, T. Nayak, A. Andreopoulos, G. Garreau, M. Mendoza, J. Kusnitz, M. Debole, S. Esser, T. Delbruck, M. Flickner, and D. Modha, "A Low Power, Fully Event-Based Gesture Recognition System," in *2017 IEEE Conference on Computer Vision and Pattern Recognition (CVPR)*, vol. 27, no. 36. IEEE, Jul. 2017, pp. 7388–7397.